A Modelica dynamic model of a supercritical CO_2 energy conversion system for EU-DEMO

S. Ferrero[1], L. Batet[2,*], J.I. Linares[3], E. Arenas[3], A. Cantizano[3], L. Savoldi[1]

[1]*MAHTEP Group, Energy Department "Galileo Ferraris" (DENERG), Politecnico di Torino, Torino, Italy*
[2] *Division of Nuclear Engineering (Department of Physics), Universitat Politècnica de Catalunya, Barcelona, Spain*
[3] *ICAI School of Engineering, Comillas Pontifical University, Madrid, Spain*

Nuclear fusion technology is one of the main valuable candidates for providing a trustable base load in low-carbon future energy scenarios, thanks to its power density, low emissions and flexibility, together with innovative power conversion systems that could improve its performance, as the supercritical CO_2 Brayton cycle. Since the nuclear plant will be required to provide variable loads, due to the fluctuating nature of renewable energies, a powerful modelling tool will be necessary to simulate different power outputs. The present paper presents a dynamic model of a supercritical CO_2 power cycle developed with Modelica, aimed at the design of control systems to adjust the power production according to the load required. Thanks to the activity of three PI controllers, the system is able to follow a variable load profile while preserving the turbomachinery inlet temperature, to avoid any possible damage of the devices. The work has shown the adequacy and potential interest of the use of Modelica in this kind of analyses.

Keywords: Supercritical CO_2 Brayton cycle, EU DEMO, Modelica, Fusion Power, Balance of Plant

Glossary

Acronym	Meaning
C	Compressor
CAPEX	Capital Expenditure
CIT	Compressor Inlet Temperature
$^{S}CO_2$	Supercritical CO2
DAE	Differential algebraic equation(s)
EES	Engineering Equation Solver
HCPB	Helium Cooled Pebble Bed
HTR	High Temperature Recuperator
HX-HTS	High Temperature Molten Salt Heat Exchanger
PC	Pre-Cooler
PCHE	Printed Circuit Heat Exchanger
PI	Proportional-Integral controller
T	Turbine
TIT	Turbine Inlet Temperature

Symbol	Meaning
a_{in}	Speed of sound at the inlet
α	Relative velocity
$e(t)$	Input signal to the controller
h_i	specific enthalpy at state point i
η_C	Compressor's efficiency
η_T	Turbine's efficiency
η_{cycle}	cycle efficiency
K_c	Gain of the controller
$\dot{m}$	Mass flow rate
N	Actual rotational velocity
p_i	Pressure at state point i
PP	Pinch point
p-v	Pressure-Specific Volume
PV	Process variable
$\dot{Q}_{HTR}$	HTR duty
$\dot{Q}_{HX-HTS}$	HX-HTS duty
$\dot{Q}_{PC}$	Pre-cooler duty
ρ_{in}	Density of fluid at the inlet
s_i	Entropy at state point i
SP	Set point value for the controller
T-s	Temperature-Entropy
T_i	Time constant of the PI
$u(t) - u_0$	Variation of the controller output
v	Relative velocity
$\dot{W}_C$	Compressor power
$\dot{W}_T$	Turbine power

1. Introduction

In the context of tackling the climate change issue [1], renewable energies are playing a key role in the transition to a future low carbon scenario, in which nuclear fusion technologies could share an important part of the demand [2] in combination with innovative energy conversion systems, like supercritical CO_2 ($^{S}CO_2$) power cycles.

So far, the most used energy conversion system is the Rankine steam power cycle, which not easily fits with the heat sources found in fusion nuclear and solar plants. An alternative to the steam cycle is the supercritical CO_2 Brayton cycle, which presents several advantages compared to the classic Rankine cycles, thanks to the peculiarities of the carbon dioxide [3]-[5]: compactness, higher efficiencies in the operating temperature ranges of advanced solar (high temperature central solar receiver) and nuclear (e.g. sodium fast reactors) power plants, no phase changes, and a manageable pinch-point problem. The high compactness, both in heat exchangers (printed circuit heat exchangers, PCHE, are used) and in turbomachines (due to the high density of CO_2 at supercritical state), leads to very low inertia, which makes it possible a good load-follow behaviour. In addition to this dynamic behaviour, the high compactness greatly reduces the footprint of the power plant and the CAPEX,

* *lluis.batet@upc.edu*

which makes this power cycle very attractive in fusion power plants.

In its supercritical state, CO_2 presents interesting properties for a fluid in an energy conversion system. Above the critical pressure (7.4 MPa) and near the critical temperature (31°C) the fluid properties become non-ideal, conferring advantages that make it a valid operative fluid; in particular, density values similar to liquids allow consistent savings in terms of compression work, operating close to the critical point. However, some potential issues arise from the closeness to the critical point: the high specific heat in these conditions leads to high cooling medium mass flow rate; moreover, near the critical point, a large difference exists between the specific heat of each stream in the recuperator, arising pinch-point issues.

Interest in $^{S}CO_2$ power cycles has been gaining momentum over the last years, and the potential of this technology also in the nuclear fusion field has been shown. Wu et al. (2020) recently published a review of the state of the art of the CO_2 application in the nuclear field, listing research activities and challenges worldwide [6]. Important investigations have been carried out also on the modelling side, focused on the definition of control strategies: Carstens (2007) developed a complete and deep study about $^{S}CO_2$ applied to IV generation nuclear reactors, testing many partial load operation strategies and suggesting the most effective [7].

Within the EUROfusion research program (Euratom Horizon 2020) [8], the convenience of using those type of cycles in the future EU-DEMO prototype plant has being extensively studied [9][10]. One of the cycles already designed, aimed at the HCPB breeding blanket, decouples the pulsed operation of the nuclear reactor from the electricity production by means of thermal energy storage in the form of molten salt sensible heat. The load-follow operation of the fusion power plant can take advantage of this isolation to maintain the operation of the reactor whereas the demand is slowed down. Steady state analyses of that cycle have been already done using the Engineering Equation Solver (EES) in order to optimize the efficiency of the cycle [11]. That design is chosen as a reference for the work presented here.

In a scenario with a large share of electricity generation from renewable sources, the balance of the grid will be achieved by means of demand-response, massive storage (pumped-hydro, batteries, hydrogen), and flexible operation of the base-load generators. The integration and operation of fusion plants in this context will require robust and flexible dynamic analysis tools.

Following the analysis by Luu et al. (2017), who used Modelica to simulate transients in a recompression $^{S}CO_2$ cycle, modelling a start-up scheme and a loss of charge accident of the plant [12], the present work focuses on the dynamic modelling of the reference CO_2 cycle, requested to follow a load profile, using the Modelica language. Modelica is an object-oriented, open source, a-causal, and multi-domain modelling language, widely used in the scientific community in the field of modelling of complex physical systems [13]. The aim of our model is the future definition of the system control strategies simulating dynamic conditions, such as variable loads, witnessing its potential and interest in further developments.

2. Methodology

2.1. Modelling toolbox

Modelica [14] has been chosen as the modeling framework to solve the problem at hand. In the past, the group at UPC has used RELAP5-3D [15] for similar purposes, but the use of an open source toolbox allows more flexibility in the modelling. Modelica aims at the modeling of systems involving several physical domains by expressing them in the form of differential-algebraic equation (DAE) systems [14].

Note that the mathematical models of complex systems, such as the one considered in the paper, can be conveniently built by aggregation of the models of their constituent parts, following a modular object-oriented modelling. Two different approaches could be followed in principle: 1) A procedural or Causal Approach, where the models are described in a form which is close to the solution algorithm and the interaction between the models is formalized in terms of input and output variables; 2) A declarative or A-Causal Approach, which is the one selected there by using Modelica, where the models are described by DAE in a context-independent form and the interaction between the models is formalized in terms of connection equations, without any need for specification on causality. In Modelica, the basic models in its object-oriented environment are highly re-usable and the overall models become much more readable than in the first case, where each sub-system model in fact depends on the selection of input and output variables at the system boundary. Furthermore, the introduction of new elements in the model, such as controllers, and the optimization of the power cycle are easily and effectively carried out within the Modelica a-causal approach, without the need of re-writing part of the model as it would have been in a classical causal approach.

The Modelica model, for the simulation of the thermal-hydraulic system here, has been developed within the Dymola platform, and relies on the availability of the libraries ThermoPower [16], ExternalMedia [17], and SolarTherm [18]. Heat exchangers have been built using ThermoPower components, in particular the water tubes. Their model is based on the dynamic equations of conservation of mass, momentum, and energy, discretizing the partial spatial derivatives with the Finite Volume method. The energy balance equation is written assuming a uniform pressure distribution; indeed, the pressure drop is lumped at the pipe's outlet. The velocity is considered uniform on the cross section. The heat conduction in the longitudinal direction is neglected, while it is allowed through the pipe wall.

On the other hand, the turbomachinery components work using performance tables, where efficiency and

pressure ratio are defined as function of the relative mass flow rate and speed.

The fluids data have been estimated using the mentioned libraries. In particular, water medium was already present in the Modelica internal library, its properties defined in the IAPWS/IF97 standard [19]. ExternalMedia [17] has been used for the CO_2 medium: this library interacts with the properties database FluidProp®. Lastly, the molten salt properties are computed in the SolarTherm library [18], created by the Astralian Solar Thermal Research Iniciative (ASTRI) program.

The solution scheme used is the DASSL code. It is an implicit, higher order, multi-step solver with the possibility to control the step-size and considered stable for a wide range of models [20].

2.2. Power cycle layout

The system has been built taking as reference an 800 MW recuperative energy conversion system designed in the frame of the H2020 EUROfusion Project [11] (Fig. 1). The heat source is a molten salt storage, which in turn is assumed heated by helium from a HCPB fusion reactor, while the cooling system has been decided to be water-based. Thus, the model of the cycle is composed by one compressor (C), one turbine (T), and three heat exchangers: precooler (PC), high temperature recuperator (HTR) and high temperature molten salt heat exchanger (HX-HTS) [11] [21].

The design parameters of the system components are listed in Table 5 below, as compared with the values obtained with the model. The performance of the components as designed is presented in Table 6, also compared with the steady state results from the model.

The cycle is provided with other components aiming at its control: an expansion vessel used to maintain a desired pressure value at the compressor's inlet, and a turbine bypass valve, used in partial load operation. The valve modelled follows an equal percentage characteristic and its parameters have been adjusted so that the valve has a balanced action on the process.

Three Proportional-Integral controllers have been included in the model, as explained in section 3.2. The layout scheme is presented in Fig. 1.

2.3. Components description

Heat exchangers

The heat exchange has been entrusted to Printed Circuit Heat Exchanger (PCHE) devices, using technical data provided by Heatric®, composed by modules 0.6 m x 0.6 m containing 96000 semicircular channels each and with variable length. They have been modelled considering straight channels made of stainless steel 316L [22][23] and parallel counter flow. According to literature, Gnielinski results to be the correlation that better evaluate the heat transfer on the carbon dioxide and molten salt sides, using the mean temperature between inlet and outlet [24][25] for the fluid thermo-physical properties. For the water side, an empirical equation was proposed by Chu et al. [26]. Moreover, in the same paper, Chu et al. suggest another empirical formulation to compute the CO_2 pressure drop in PCHEs.

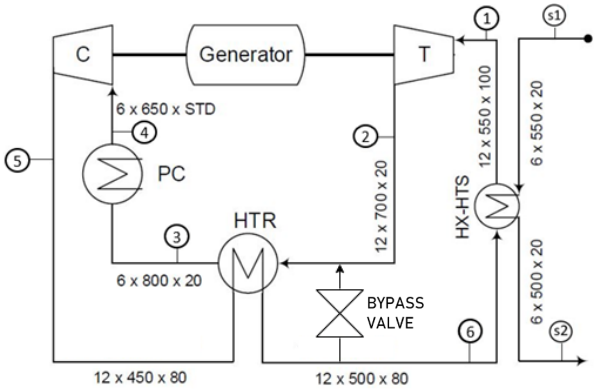

Fig. 1. Scheme of the reference cycle. S1 and S2 are respectively the molten salt inflow and outflow.

Turbomachinery

The turbomachines have been modelled making use of performances tables, function of relative speed and flow rate; in particular, the compressor tables have been developed at Comillas University. In Fig 2 it is possible to observe the compressor's performance maps, function of α, relative velocity, and ν, relative mass flow rate, displayed in Equations 1 and 2, where $\dot{m}$ is the mass flow [kg/s], ρ_{in} the density [kg/m^3,] a_{in} the speed of sound [m/s] and N the device velocity [rpm].

$$\alpha = \frac{N}{a_{in}} \Big/ \left(\frac{N}{a_{in}}\right)_{rated} \qquad \text{(Eq. 1)}$$

$$\nu = \frac{\dot{m}}{\rho_{in} a_{in}} \Big/ \left(\frac{\dot{m}}{\rho_{in} a_{in}}\right)_{rated} \qquad \text{(Eq. 2)}$$

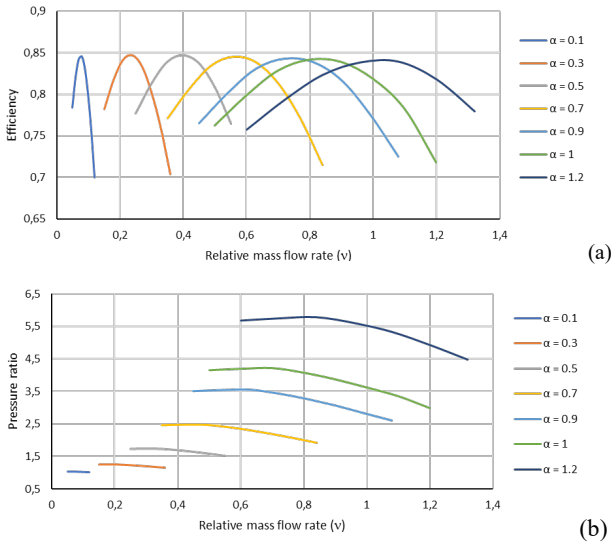

Fig 2. Performance maps of the compressor as modelled: (a) compressor efficicency; (b) Compressor pressure ratio.

On the other hand, the turbine was derived from the work of Moisseytsev et al. [27] (Fig. 3).

Controllers

The control system is formed simply by 3 PI controllers, acting respectively on the flow rates of water, molten salt and the bypass valve aperture. The first two PIs act in order to make the system operate at the nominal conditions, controlling the temperatures at the compressor's inlet and at the turbine inlet respectively. The last controller acts on the bypass valve, that connects the cold side outlet with the hot side inlet of the HTR, regulating its aperture and, consequently, the bypassed flow and the power output.

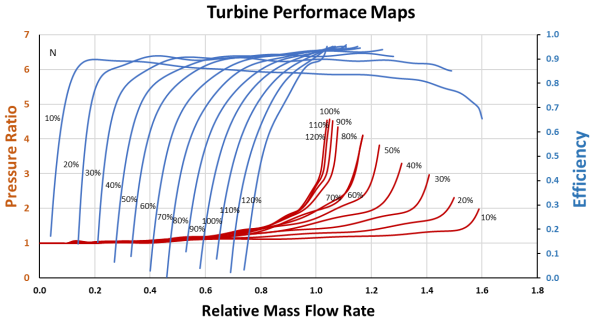

Fig. 3 Reference turbine's performance map based on [27]. Values are expressed as function of relative mass flow rate and relative speed N.

The PI response is regulated by the following equation (Eq. 3):

$$u(t) - u_0 = K_c\, e(t) + \frac{K_c}{T_i} \int_0^t e(t)dt \qquad \text{(Eq. 3)}$$

with *u(t)* being the output of the controller and u_0 the initial output value. The PI action depends on the measured error from the set point, defined as difference between the set point value (SP) and the real value of the variable measured, called process variable PV (Eq. 4).

$$e(t) = SP - PV \qquad \text{(Eq. 4)}$$

The PI is characterized then, by the gain K_c, and the integral time constant T_i. But also, according to the component controlled, the error and output assume different physical meanings, measuring and acting on different variables that may differ also on the units of measure. Table 1 sums up the $K_c - T_i$ values and lists the physical variables handled in each controller.

Table 1 Controllers definition

Controller name	Output $u(t)$	Error $e(t)$	Kc	T_i (s)
Water PI	Water mass flow [kg/s]	Compressor inlet temp. [°C]	-3914.09	28.6
Molten Salt PI	Molten salt mass flow [kg/s]	Turbine inlet temp. °C]	5.3176	6.65
Valve PI	Bypass valve aperture [%]	Reduction in power output [MW]	5.24E-11	0.9

Mass flow controllers have been adjusted after analysing the system response to a step variation of the water flow and molten salts flow respectively. The procedure is described in Ferrero [21].

Bypass valve deserves a special comment: the control output should be applied to the velocity of the valve actuator, not to the valve opening. An approximation has been taken here using a pure integral controller acting on the valve position, as an approximation of a proportional controller acting on the actuator's velocity (eq. 5).

$$u(t) - u_0 = \frac{K_c}{T_i} \int_0^t e(t)dt \qquad \text{(Eq. 5)}$$

This controller has been adjusted by performing a step opening of the valve and observing the response of the system, but a large deal of trial an error has been needed.

2.4. Model layout

Fig. 4 represents the layout of the model as implemented in Modelica. The model solves the conservation equations for 179 nodes (control volumes), of which 127 correspond to the CO_2 circuit, 27 to the molten salts circuit, and 22 to the water circuit. In total there are 67 slabs where heat is exchanged between two streams of fluids (HTR: 25, HX-HTS: 23, PC: 19). This implies solving around 12000 equations with the same number of unknowns. The nodes solved for each of the components are shown in Table 2. A grid independency study was performed before choosing the number of nodes for the heat exchangers (details in Ferrero [21]). For the pipes, each node corresponds roughly to 10 m, though it is not relevant, giving the fact that the model concentrates the pressure losses at the pipes' outlet.

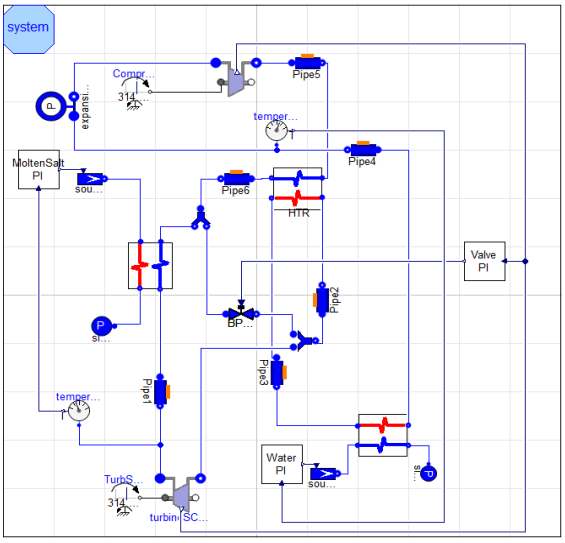

Fig. 4. Layout of the model as implemented in Modelica

Table 2. Number of nodes selected for each component of the model

Component	Nodes	Component	Nodes
CO_2 circuit		**Molten salts circuit**	
Pipe 1	10	HTS Hot side	25
Turbine	1	Molten salts source	1
Pipe 2	3	Molten salts sink	1
HTR Hot Side	25		
Pipe 3	3	**Water circuit**	
PC Hot Side	19	PC Cold Side	20
Pipe 4	3	Water source	1
Compressor	1	Water sink	1
Pipe 5	7		
HTR Cold Side	25		
Pipe 6	7		
HTS Cold Side	23		
Expansion tank (ideal)	1		

3. Results

3.1. Steady-state operation

The simulated system was firstly run in static (uncontrolled) conditions with fixed inlet temperatures and mass flows of molten salt and water. In order to have a first validation of the Modelica model, its results have been compared to the design values, which were obtained by Comillas [11], solving the equations in Table 3 with the EES [28] and are shown in Table 4 and Fig. 5. Property data was supplied to the EES solver as built-in functions, based on the fundamental equation of state developed by R. Span and W. Wagner [29]. The benchmark showed good accordance of results, witnessing the correctness of the model construction, characterized by a CO_2 flow of about 7000 kg/s and a cycle efficiency of 37.8%.

Table 3. Equations solved with EES to get the design values of the system. Subscripts refer to the points labelled in Fig. 1.

Compressor	$\dot{W}_C = \dot{m} \cdot (h_5 - h_4)$ $\eta_C = \frac{h(p_5, s_4) - h_4}{h_5 - h_4}$
Turbine	$\dot{W}_T = \dot{m} \cdot (h_1 - h_2)$ $\eta_T = \frac{h_1 - h_2}{h_1 - h(p_2, s_1)}$
HTR	$\dot{Q}_{HTR} = \dot{m} \cdot (h_2 - h_3)$ $h_2 - h_3 = h_6 - h_5$ $PP = T_3 - T_5$
HX-HTS	$\dot{Q}_{HX-HTS} = \dot{m} \cdot (h_1 - h_6)$
PC	$\dot{Q}_{PC} = \dot{m} \cdot (h_3 - h_4)$
Cycle efficiency	$\eta_{cycle} = \frac{(h_1 - h_2) - (h_5 - h_4)}{(h_1 - h_6)}$

Table 4. Comparison of the performance of the components of the system simulated in Modelica (uncontrolled steady state) with the design values [11].

Component	Design	Model
$\dot{W}_C$ [MW]	240	305
$\dot{W}_T$ [MW]	1047	1063
$\dot{Q}_{HX-HTS}$ [MW]	2029	2063
$\dot{Q}_{HTR}$ [MW]	2183	2141
$\dot{Q}_{PC}$ [MW]	1223	1283
η_{cycle}	39.8%	37.8%

However, minor discrepancies arose due to some differences between the two cycles. Indeed, in the EES model, local pressure drops at heat exchangers' inlets/outlets and the pressure losses along the piping were not considered, while the present work includes also them. Moreover, the turbomachinery used here has lower efficiencies compared to ones in the EES cycle. Fig. 5 shows the T-s and p-v diagrams of the cycles, from where the similar operating conditions in the two cases can be noticed. Differences can be observed at the compressor outlet, where a higher outlet temperature and pressure was computed with Modelica, caused both by the more consistent circuit pressure losses and different turbomachinery operation.

Differences also arise from the fact that the inlet temperature of compressor and turbine in the simulation are slightly different than those considered in the design (35.6°C vs. 35.0°C and 489.7°C vs. 490°C respectively).

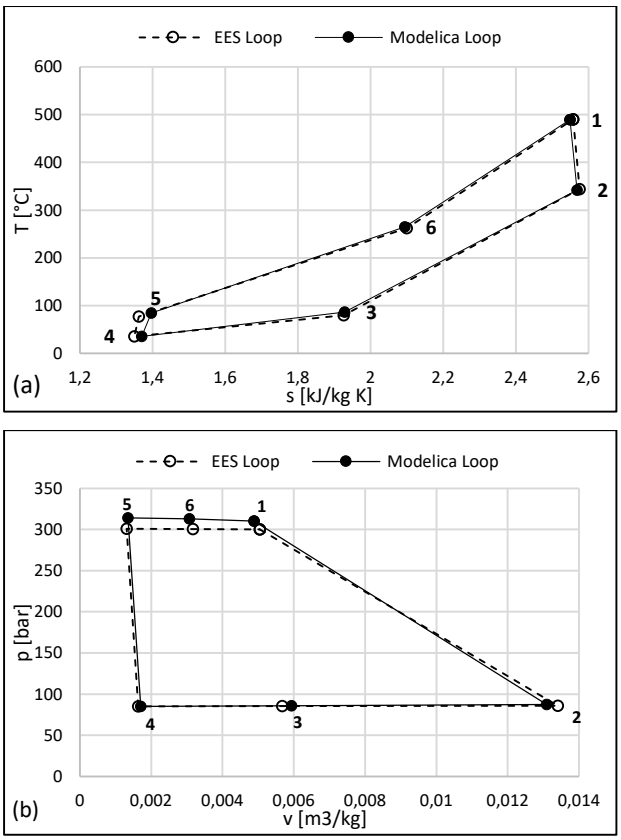

Fig. 5. Steady-state analysis: a) T-s and b) p-v diagrams of Comillas University [11] (dashed lines) and Modelica (this work, solid lines) uncontrolled static process. The numbering refers to Fig. 1.

3.2. Dynamic analysis

The differences found in Table 4 and Fig. 5 can be further reduced by regulating the mass flow rates of molten salt and water, adding two PI controllers, respectively in the HX-HTS and PC, targeting the design inlet temperatures. Table 5 compares the design parameters of the system with the values either implemented in the model or obtained in the controlled steady state simulation. Table 6 shows the comparison between the design and the steady state simulation once the controls are in place. It can be observed how the performance of the components is better predicted that in the uncontrolled run (Table 4). The efficiency of the thermodynamic cycle is also improved since it was designed to optimize the efficiency for those values [11]. Nevertheless, some differences persist. It must be taken into account that, in the reference process, turbomachinery has a fixed efficiency and pressure ratio, whilst the Modelica model uses more realistic devices. For instance, the difference observed at the compressor outlet (state 5 in Table 6), where a higher outlet temperature can be identified, is caused both because the pressure ratio must be higher to overcome the more realistic pressure losses of the model as compared to the design, but also to a lower efficiency of the component against the one used by Comillas.

Table 5 Comparison of the system design parameters used by Comillas [11] with the controlled model steady state results.

Component	Design	Model
Compressor		
Efficiency [%]	88.0	80.7
Turbine		
Efficiency [%]	93.0	93.7
HTR		
Minimum Temperature Approach [°C]	3.0	2.3
Volume [m^3]	142.2	148.5
Pressure drop (hot stream) [kPa]	40	170
Pressure drop (cold stream) [kPa]	40	112
HX-HTS		
Minimum Temperature Approach [°C]	5.0	5.0
Volume [m^3]	359.3	324.5
Pressure drop (CO_2) [kPa]	40	280
Pressure drop (Salt) [kPa]	60	28
PC		
Minimum Temperature Approach [°C]	5	5
Volume [m^3]	31.91	34.32
Pressure drop (CO2) [kPa]	40	71
Pressure drop (water) [kPa]	500	120

Table 6. Comparison between design performance [11] and simulation at controlled steady state condition with Modelica.

	Design		Modelica	
$\dot{W}_C$ [MW]	240.1		264.6	
$\dot{W}_T$ [MW]	1046.9		1038.6	
$\dot{Q}_{HX-HTS}$ [MW]	2029.4		2006.2	
$\dot{Q}_{HTR}$ [MW]	2182.7		2175.4	
$\dot{Q}_{PC}$ [MW]	1222.6		1232.2	
η_{cycle}	39.76%		38.58%	
CO_2 mass flow rate [kg/s]	6912		6902	
Molten salt mass flow rate [kg/s]	6185		6088	
Cooling water mass flow rate [kg/s]	29297		32034	
CO_2 state points	**T [°C]**	**p [bar]**	**T [°C]**	**p [bar]**
1	490.0	300.0	490.0	299.7
2	343.8	85.8	344.9	87.4
3	79.6	85.4	80.9	85.7
4	35.0	85.0	35.0	85.0
5	76.6	300.8	78.6	303.6
6	262.2	300.4	264.6	302.5

Once these temperature control systems are active, the system is able to sustain other transients while preserving the turbomachinery activity and integrity. With these controls in place and with the aim of testing the performance of the model in more demanding transients, a dynamic simulation has been carried out in which it has been assumed (as an example) that the system power output is required to follow the load profile represented in

Fig. 6. It is characterized by a first 30% reduction of power in 15 minutes, followed by a constant period of 30 minutes, ending with a slight increase 15 minutes long, up to the 85% of the nominal value. The task is carried out by a third controller, which adjusts the bypass valve aperture and, consequently, the system power output.

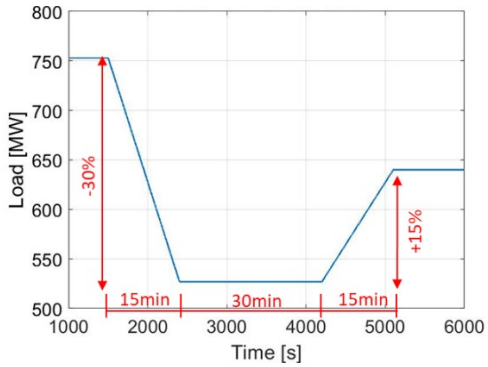

Fig. 6. Requested load profile used in the simulation

The three controllers have been activated one by one, letting the system stabilizing after each activation. Fig. 7 represents the time sequence of activations.

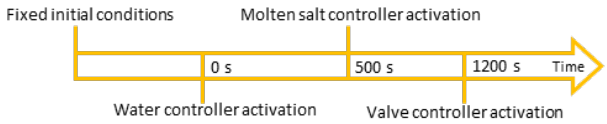

Fig. 7. Dynamic simulations timeline

Water and Molten salt control

The first two PI controllers have been set for the specific purpose of regulating the molten salt and water mass flow rates to fix the inlet temperatures of turbine and compressor, respectively at 490°C and 35°C. The controllers are activated in series.

First, the precooler water flow controller is activated at the time zero, taking the Compressor Inlet Temperature (CIT) from 35.7°C to 35°C in 200 seconds, thanks to a 9.92% increase of the water flowing in the heat exchanger. This procedure improves also the compressor performance, from 76.8% to 80.7%. Fig. 8 shows the CIT trend at the controller activation moments.

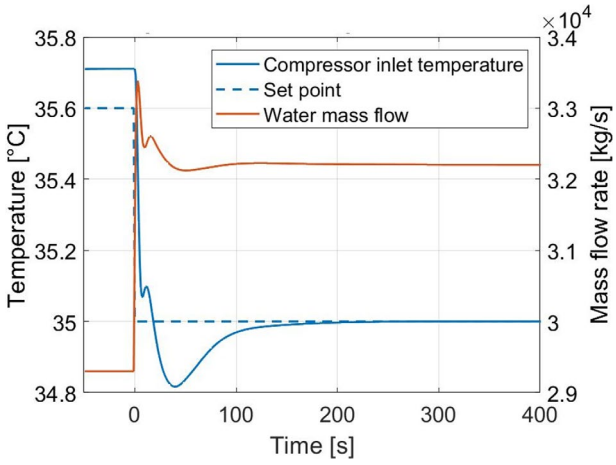

Fig. 8. Dynamic analysis: Compressor inlet temperature evolution after the control activation

After the system stabilization, at the 500th second also the molten salt flow controller is activated, aiming at the regulation of the Turbine Inlet Temperature (TIT), decreasing it from 491.1°C to 490°C, reducing the salt flow by 2.5%. In this case, the device efficiency remains almost stable, since the efficiency curves are approximately flat close to that operation point. The control system acts slower compared to the previous, due to the large size and inertia of the HX-HTS, requiring about 600 seconds to reach the set point. This is noticeable also comparing the delay of about 100 seconds between the two curves in Fig. 9, time required by the thermal information to reach the turbine inlet. That behavior justifies a more conservative control activity, that otherwise would cause oscillations and eventually damages in a real device. Further in the CO_2 circuit, the temperature variation is transmitted to the PC, where the water controller reacts, adjusting the water flow to maintain the CIT stable.

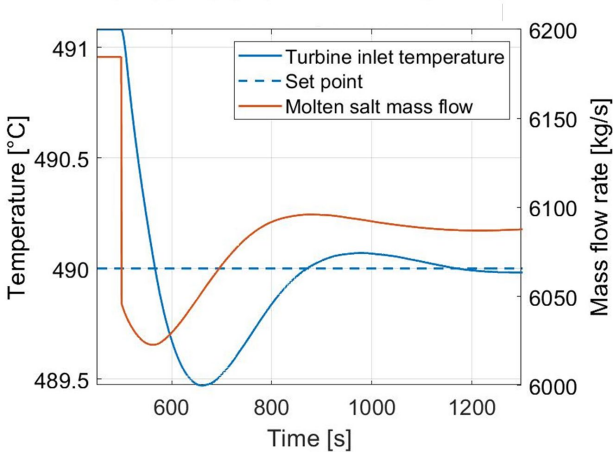

Fig. 9. Turbine Inlet Temperature evolution at the control system activation

Partial load operation

The bypass valve that has been maintained closed in all the other simulations, can now be used to control the partial load operation of the plant, for example during periods of higher renewables production. The valve allows the flow to skip both the turbine and the HX-HTS; this position is suggested by Carstens and preferred to the bypass of only the turbine [7]. A third PI has been sized and inserted in the model to control the valve opening, according to the power output required. Indeed, the simulated plant has been requested to follow the load profile described above (Fig. 6), also shown with the dashed line in Fig. 11. The ramp rates are 15 MW/min down and 7.5 MW/min up approximately, which are values aligned with the present load-following capabilities of present thermal and nuclear plants [30].

During the ramp, it is assumed that turbomachines are operated at constant speed (i.e., are assumed to be connected to an infinite bus). The control used simply compares the desired load profile with the actual electricity generation and acts consequently opening or closing the bypass valve. The pressure at the discharge of the turbine increases during the load rejection transient, but in a limited form (0.5 bar at the end of the ramp down), because of the action of the expansion tank downstream of the PC. Thanks to the activity of the controllers the turbine's performance variation is small (Fig. 10). The relative numbers variation remains limited to just about 1% during the simulation (approximately α=1.01, ν=1.03), and so the turbine's efficiency is almost constant. This behaviour can be understood looking at Fig. 3. (the efficiency curves are almost flat).

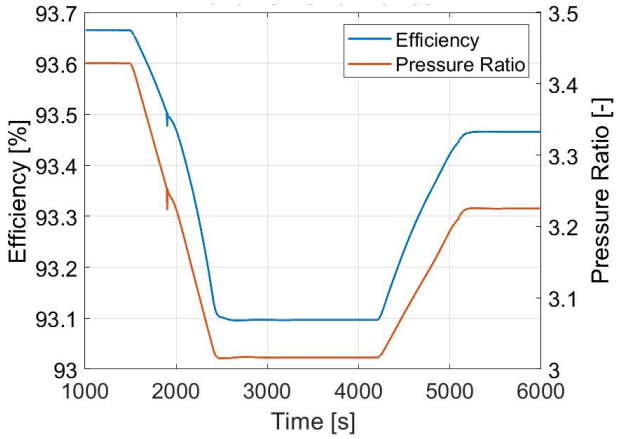

Fig. 10. Variation of the turbine's efficiency and pressure ratio during the partial load operation transient.

The control system shows good reactivity, without appreciable oscillations and managing to follow the profile very accurately at the beginning, and with just around 100 seconds of delay when the two ramps end. Fig. 11 represents the behavior just described, showing the load profile and the system power output, together with the valve opening.

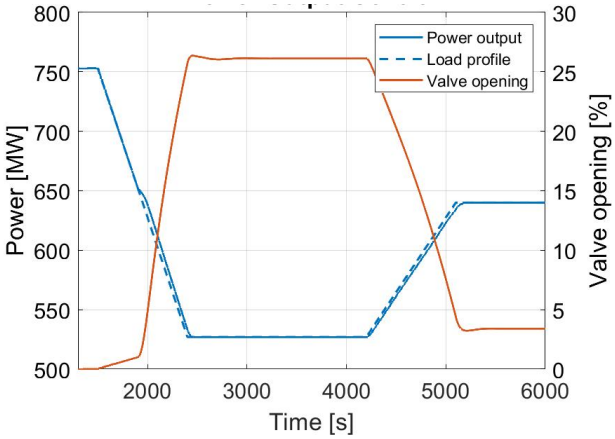

Fig. 11. Power output control activity.

It can be interesting to look at the behaviour of other variables. The compressor discharge pressure decreases during the transient (Fig. 12), since the mass flow circulating through it increase up to more than 7700 kg/s at the end of the ramp down. Consequently, the compressor pressure ratio and efficiency values are reduced (according to Fig 2). The same graph shows also the HTR low pressure side inlet temperature: the more the valve is opened, the bigger amount of fluid skips the HTS and cannot be heated up. Thus, mixing it with the fluid discharged by the turbine, the resulting temperature at the HTR inlet appears lowered.

The greater mass flow rate through the compressor along with the drop in its efficiency translate into a higher compression power required. Even when there is a reduction of the CO_2 flow rate through the HX-HTS, which means lower ingress of heat in the CO_2 circuit, the efficiency (expressed as electric power over energy absorbed by the CO_2 in the HX-HTS) decreases dramatically, down to 28.2% from 37.5% (Fig. 13).

It must be reminded also that the HX-HTS controller is adapting the molten salt flow in order to keep the TIT fixed and avoid peaks of temperature at the turbine inlet due to the smaller amount of CO_2 crossing the device, protecting it from possible damages. This control in the molten salt stream of HX-HTS does not imply that the molten salt which removes the heat from the reactor varies, due to the presence of hot and cold molten salt tanks, which isolate the reactor cooling loop from the CO_2 power cycle. In fact, such thermal energy storage system, required to manage the pulsed operation of the tokamak, allows the constant operation of the reactor in pulse period, simply oversizing the tanks to store the excess thermal power from the reactor in periods of low electricity demand.

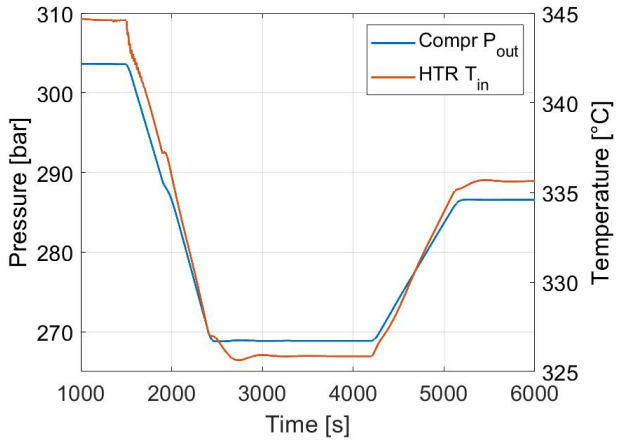

Fig. 12. Compressor discharge pressure and temperature at the low pressure (hot) side inlet to HTR during the transient

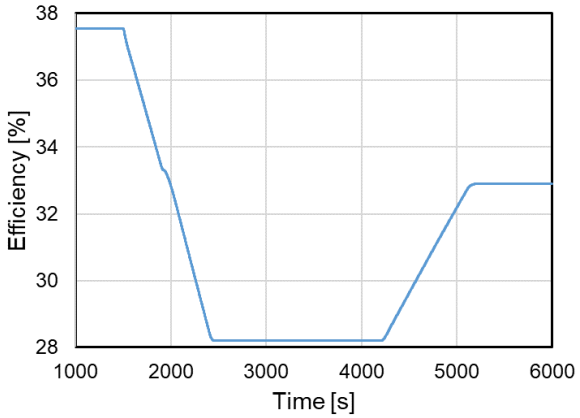

Fig. 13. Variation of the efficiency of the power conversion system, including mechanical efficiency, during the partial load operation

4. Conclusions

In the framework of the dynamic modelling of a supercritical CO_2 energy conversion system, connected to a fusion nuclear power plan, effective and precise control strategies have been developed using Modelica, and shown to be capable to maintain optimal operating conditions and manage the power output. Modelica has proved to be a convenient modelling language for the dynamic simulation of power conversion systems.

A $^{S}CO_2$ power cycle model has been built based on and benchmarked against previous results in steady state operation. Two of the PI controllers included in the model act on the water and molten salt flows, adjusting the temperature at the turbomachinery inlets, helping to prevent damages, preserve the critical fluid conditions, and retain high efficiencies of the devices. In order to test the performance of the model under transient conditions, a variable load profile over a time range of one hour (that could be representative of the flexible plant operation with variable renewables production) has been used to trigger the dynamic response of the system. With this aim, a third controller acting over the bypass valve has been implemented, with a fairly good result.

In perspective, the results obtained are encouraging for further developments and refinements of the controls, and for upgrading the model to simulate more complex systems, and also to target different operating conditions, including highly variable and cyclic dynamic loads.

Acknowledgments

This work has been carried out within the framework of the EUROfusion Consortium and has received funding from the Euratom research and training programme 2014-2018 and 2019-2020 under grant agreement No 633053. The views and opinions expressed herein do not necessarily reflect those of the European Commission.

References

[1] Intergovernmental Panel on Climate Change (IPCC), 2018: Summary for Policymakers. In: Global Warming of 1.5°C. An IPCC Special Report on the impacts of global warming of 1.5°C above pre-industrial levels and related global greenhouse gas emission pathways, in the context of strengthening the global response to the threat of climate change, sustainable development, and efforts to eradicate poverty [Masson-Delmotte, V., P. Zhai, H.-O. Pörtner, D. Roberts, J. Skea, P.R. Shukla, A. Pirani, W. Moufouma-Okia, C. Péan, R. Pidcock, S. Connors, J.B.R. Matthews, Y. Chen, X. Zhou, M.I. Gomis, E. Lonnoy, T. Maycock, M. Tignor, and T. Waterfield (eds.)]. World Meteorological Organization, Geneva, Switzerland, 32 pp. https://www.ipcc.ch/sr15/chapter/spm/.

[2] H. Cabal, Y. Lechón, C. Bustreo, F. Gracceva, M. Biberacher, D. Ward, D. Dongiovanni, P.E. Grohnheit, Fusion power in a future low carbon global electricity system, Energy Strategy Reviews. 15 (2017), 1-8. https://doi.org/10.1016/j.esr.2016.11.002.

[3] G. Angelino (1968). "Carbon Dioxide Condensation Cycles For Power Production." ASME. J. Eng. Power. 1968; 90(3): 287–295. https://doi.org/10.1115/1.3609190.

[4] V. Dostal, M.J. Driscoll, P. Hejzlar (2004). A Supercritical Carbon Dioxide Cycle for Next Generation Nuclear Reactors. March 10, 2004. MIT-ANP-TR-100. https://web.mit.edu/22.33/www/dostal.pdf

[5] Y. Liu, Y. Wang, D. Huang, Supercritical CO2 Brayton cycle: A state-of-the-art review, Energy. 189 (2019) 115900. https://doi.org/10.1016/j.energy.2019.115900.

[6] P. Wu, Y. Ma, C. Gao, W. Liu, J. Shan, Y. Huang, J. Wang, D. Zhang, X. Ran, A review of research and development of supercritical carbon dioxide Brayton cycle technology in nuclear engineering applications, Nuclear Engineering and Design. 368 (2020) 110767.

[7] N.A. Carstens, Control Strategies for Supercritical Carbon Dioxide Power Conversion Systems, MIT, 2007. https://dspace.mit.edu/handle/1721.1/41295.

[8] EUROfusion, EUROfusion Roadmap, Euro-Fusion.Org. (2018). https://www.euro-fusion.org/eurofusion/roadmap/.

[9] J.I. Linares, L.E. Herranz, B.Y. Moratilla, I.P. Serrano, Power conversion systems based on Brayton cycles for fusion reactors, Fusion Engineering and Design. 86 (2011) 2735–2738. https://doi.org/10.1016/j.fusengdes.2011.02.010.

[10] J.I. Linares, A. Cantizano, B.Y. Moratilla, V. Martín-Palacios, L. Batet, Supercritical CO2 Brayton power cycles for DEMO (demonstration power plant) fusion reactor based on dual coolant lithium lead blanket, Energy. 98 (2016) 271–283. https://doi.org/10.1016/j.energy.2016.01.020.

[11] J.I. Linares, A. Cantizano, E. Arenas, M. Carmona, J. Parrondo, B.Y. Moratilla, J. Porras, Ll. Batet, J.M. Sojo, (2018). Alternative PCS based on Brayton Supercritical CO2 for HCPB. 31 January 2018. IDM reference: EFDA_D_2MGGL5.

[12] M.T. Luu, D. Milani, R. McNaughton, A. Abbas, Dynamic modelling and start-up operation of a solar-assisted recompression supercritical CO 2 Brayton power cycle, Applied Energy. 199 (2017) 247–263. https://doi.org/10.1016/j.apenergy.2017.04.073.

[13] F. Casella & A. Leva (2006) Modelling of thermo-hydraulic power generation processes using Modelica, Mathematical and Computer Modelling of Dynamical Systems, 12:1, 19-33, https://doi.org/10.1080/13873950500071082.

[14] S.E. Mattsson, H. Elmqvist, M. Otter, Physical system modeling with Modelica, Control Engineering Practice, Volume 6, Issue 4, 1998, Pages 501-510, ISSN 0967-0661, https://doi.org/10.1016/S0967-0661(98)00047-1.

[15] L. Batet et al., Modelling of a supercritical CO2 power cycle for nuclear fusion reactors using RELAP5–3D, Fusion Engineering and Design, Volume 89, Issue 4, 2014, Pages 354-359, https://doi.org/10.1016/j.fusengdes.2014.03.018.

[16] F. Casella, A. Leva, Modelica open library for power plant simulation: Design and experimental validation, Proc. 3rd Modelica Conference. (2003).

[17] F. Casella, C. Richter, ExternalMedia: A Library for Easy Re-Use of External Fluid Property Code in Modelica ExternalMedia: A Library for Easy Re-Use of External Fluid Property Code in Modelica, Proceedings 6th International Modelica Conference. (2010).

[18] Alberto de la Calle, Jim Hinkley, Paul Scott, John Pye, SolarTherm: A New Modelica Library and Simulation Platform for Concentrating Solar Thermal Power Systems, (2018).

[19] IAPWS, R7-97(2012), Revised Release on the IAPWS Industrial Formulation 1997 for the Thermodynamic Properties of Water and Steam (The Revision only Relates to the Extension of Region 5 to 50 MPa) (2007). Available at http://www.iapws.org.

[20] Petzold, L R., Description of DASSL: a differential/algebraic system solver. United States: N. p., 1982. Web.

[21] S. Ferrero, Modelica dynamic modeling of a supercritical CO2 loop for solar and nuclear applications, Politecnico di Torino, 2020. https://webthesis.biblio.polito.it/14044/.

[22] Southall, D., S.J. Dewson, Innovative Compact Heat Exchangers, Proceedings of ICAPP '10, San Diego, (2010) https://www.heatric.com/app/uploads/2018/04/Innovative-compact-heat-exchangers.pdf.

[23] AZoM, Stainless Steel Grade 316L Properties, Fabrication and Applications (UNS S31603), (2004). https://www.azom.com/article.aspx?ArticleID=2382.

[24] L. Chai, S.A. Tassou, Numerical study of the thermohydraulic performance of printed circuit heat exchangers for supercritical CO2 Brayton cycle applications, Energy Procedia. 161 (2019) 480–488. https://doi.org/10.1016/j.egypro.2019.02.066.

[25] V. Ariu, Heat exchanger analysis for innovative molten salt fast reactor, ETH, 2014.

[26] W. Chu, X. Li, T. Ma, Y. Chen, Q. Wang, Experimental investigation on SCO2-water heat transfer characteristics in a printed circuit heat exchanger with straight channels, International Journal of Heat and Mass Transfer. 113 (2017) 184–194. https://doi.org/10.1016/j.ijheatmasstransfer.2017.05.059.

[27] A. Moisseytsev, K.P. Kulesza, J.J. Sienicki, Control system options and strategies for supercritical CO2 cycles., 2009. https://doi.org/10.2172/958037.

[28] Klein SA, Nellis GF. Mastering EES, F-Chart Software, edition 63. http://www.fchartsoftware.com/ees/mastering-ees.php

[29] R. Span and W. Wagner, "A new Equation of State for Carbon Dioxide Covering the Fluid Region from the Triple-Point to 1100 K at Pressures up to 800 MPa", J. Phys. Chem., Ref. Data. Vol. 25, No. 6, 1996.

[30] IAEA. Non-baseload Operation in Nuclear Power Plants: Load Following and Frequency Control Modes of Flexible Operation. IAEA Nuclear Energy Series. No. NP-T-3.23. 2018.